Combustion and Flame 164 (2016) 126–136

Contents lists available at ScienceDirect

Combustion and Flame

journal homepage: www.elsevier.com/locate/combustflame

Parametric investigation of water loading on heavily carbonaceous syngases

Daniel G. Pugh[a,b,*], Andrew P. Crayford[a,b], Philip J. Bowen[a,b], Mohammed Al-Naama[a]

[a] Cardiff School of Engineering, Cardiff University, Wales, UK
[b] Gas Turbine Research Centre, Margam, Wales, UK

ARTICLE INFO

Article history:
Received 8 July 2015
Revised 6 November 2015
Accepted 9 November 2015
Available online 19 December 2015

Keywords:
Laminar flame speed
Converter gas
Humidity
Reaction mechanism
Experimental uncertainty

ABSTRACT

An outwardly propagating spherical flame was used to characterise the influence of water loading on the premixed combustion of an applied high CO/H_2 ratio syngas fuel blend (converter gas). A nonlinear extrapolative technique was used to obtain values of laminar flame speed for combustion with air, for varying temperature, pressure and equivalence ratio. With increased attention given to the accurate measurement of laminar flame speed, a concerted effort was made to quantify experimental uncertainty, and a detailed methodology is presented. Change in relative humidity was shown to have a substantial impact on laminar flame speed for the syngas, increasing measured values by up to 70% from the driest cases. This observed increase results from the dissociative influence of H_2O addition, and enhancement in the formation of chain carriers that catalyse CO oxidation, increasing net heat release rate. In addition to relative humidity, the decoupled influences of initial temperature and pressure were investigated parametrically; holding the mass ratios of fuel and H_2O constant for a step change in condition. Temperature rise was shown to enhance H_2O induced acceleration, with greater relative change in heat release rate for a corresponding drop in flame temperature, and the opposite effect observed for increased pressure. The effect of water addition was shown to be non-monotonic, with flame speed reduction achieved at the highest water loadings for the hottest tests, and discussed as a function of initial CO/H_2 ratio. Attention was given to the dominant reaction kinetics, with the performance of several published reaction mechanisms evaluated against experimental data using CHEMKIN-PRO; with flame speed consistently overpredicted when H_2O was added to the mixture. A modified reaction mechanism is presented for the humidified combustion of high CO/H_2 mixtures, changing the rate parameters of two chain branching reactions to give higher relative indeterminate H_2O formation, and a reduction in OH carriers. Results obtained using the modified mechanism demonstrate improved agreement with all experimental data presented here and from a previous study, including changes in H_2O concentration at elevated temperatures and pressures. The results also highlight relative humidity as a potential source of error in the experimental measurement of u_L, significant for fuels comprising large CO fractions, but also potentially for other gaseous fuels, emphasising that relative humidity should be carefully considered when comparing experimental data.

1. Introduction

The influence of water content on syngas combustion is becoming an increasingly prominent area of research, as engineers strive for the application of alternative fuels in cleaner, more efficient and complex technologies [1–5]. Central to this development is the compound chemical influence that water can have catalysing CO oxidation, in competition with a lowering of adiabatic flame temperature: Direct formation of CO_2 from CO is slow due to a high activation energy, and the presence of hydrogen facilitates chain branching OH formation, changing the dominant path for oxidation [6]. Water addition can therefore provide a non-monotonic influence on premixed flame propagation, with lower concentrations catalysing oxidation through disassociation, whilst higher concentrations will eventually dilute the reaction and temperature as the accelerative influence is lost. The work presented employs a heavily carbonaceous syngas (Basic Oxygen converter gas, which typically comprises 50–80% CO, 10–18% CO_2, 1–3% H_2 in a balance of N_2 (%vol) [7]) as a case study for detailed parametric investigation of this behaviour. It represents a practical fuel which is increasingly used throughout the industrialised world [7].

* Corresponding author at: Cardiff School of Engineering, Cardiff University, School of Engineering, Queens Buildings, The Parade, Cardiff, CF24 3AA.
E-mail address: pughdg@cardiff.ac.uk (D.G. Pugh).

http://dx.doi.org/10.1016/j.combustflame.2015.11.009

Nomenclature

A	area
A_a	pre-exponential factor
A_A, B_A, C_A	Antoine equation coefficients
E_a	activation energy
k_f	rate constant
Ka_{mid}	Karlovitz number normalised midpoint stretch rate
L_b	Markstein length
Le	Lewis number
m_f	mass of fuel
m_o	mass of oxidiser
Ma_{lin}	Markstein number representing slope of flame speed on stretch
P	initial pressure
r_{sch}	schlieren flame radius
R_{Sn}	uncertainty in regression
S_u	unstretched flame speed
S_n	stretched flame speed
t	time
T	initial temperature
T_{AD}	adiabatic flame temperature
u_L	laminar flame speed
U_{uL}	uncertainty in laminar flame speed
U_{Su}	uncertainty in unstretched flame speed
v_i	independent variable
x_f	molar fuel fraction
X	normalised condition
y_i	fixed error in variable
α	flame stretch-rate
η	mass Ratio
θ	gaseous Impurity
ρ_b	density of the burned gas
ρ_u	density of the unburned gas
σ_{Su}	standard deviation in S_u
ϕ	equivalence ratio

Subscripts

A, B, C	mass ratio identifiers

1.1. Aim

The laminar flame speed (u_L), sometimes referred to as laminar burning velocity, or burning rate, represents one of the most important fundamental physiochemical properties of a fuel mixture. It is often used as input to detailed combustion models or to validate chemical reaction mechanisms [8]. Previous work [9] undertaken by the authors and presented in Fig. 1, quantified the non-monotonic changes in u_L possible from variation in relative humidity, as a function of H_2/CO ratio for another heavily diluted carbonaceous by-product fuel (note that 0.75 g $H_2O \approx$ 72% RH at 303 K, and model predictions were generated using different reaction mechanisms in CHEMKIN-PRO). Due to the dilute nature of this fuel blend, detailed investigation was problematic given the small changes in flame speed realised from water addition, relative to experimental uncertainty.

The aim of the presented work was to experimentally investigate the influence of water content with the combustion of a practical fuel mixture comprising a higher CO fraction. Variation in air/fuel ratio was analysed, in addition to parametric studies of the influence of initial temperature and pressure. Particular attention was afforded to changes in intermediate chemistry and reactant thermo-diffusivity through the analysis of several chemical models and quantification of the burned gas Markstein Length (L_b). Experimental data were attained using an outwardly propagating spherical flame configuration,

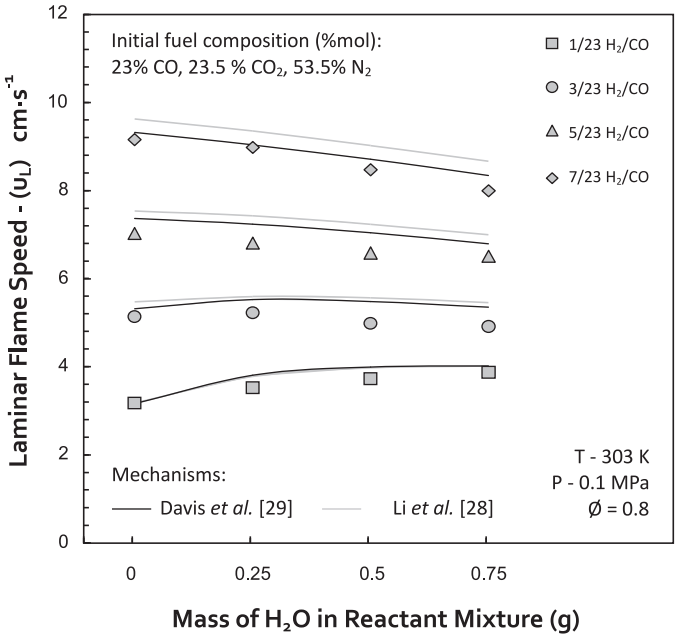

Fig. 1. Experimental (symbols) and modelled changes in laminar flame speed of humidified blast furnace gas mixtures, for combustion with air [9].

within a constant-volume combustion bomb (CVCB) which has been fully characterised previously [10].

Results were used to adapt and develop an existing chemical reaction mechanism, improving the comparative performance in modelling humidified syngas mixtures. A detailed methodology for estimating experimental uncertainty was also employed in this study, and is presented alongside the results.

2. Experimental setup

2.1. System overview

A schematic overview of the experimental setup employed is shown in Fig. 2. The CVCB has an internal volume of approximately 34 L (internal diameter: 260 mm), designed to allow for a sufficiently long experimental time window in the constant pressure region of flame expansion [10]. A PID control system regulates the ambient reactant temperature (T). Four diametrically opposed 100 mm quartz viewing windows facilitate high-speed imaging of flame propagation, by employing the widely used schlieren optical technique [10–14]. Images were captured by a CCD high-speed camera (Photron FASTCAM APX-RS (±0.05%)) at a rate of 5,000 fps. The system allowed for a spatial resolution of ~0.14 mm per pixel, with propagation rates calculated by bespoke software employing commercially available edge-detection algorithms.

H_2O was injected into the evacuated system through a self-sealing septa (see Section 2.2), with the liquid mass measured on a high-precision balance (Mettler Toledo AE50 (±0.2 mg), resolution 0.1 mg). Gaseous fuel and air were then introduced into the chamber using multiple mass flow controllers (Bronkhorst mini CORI-FLOW devices (±0.5% Rd)). The total mass required for each reactant was pre-programmed, enabling both controllers to supply batch controlled mass up to the desired value. Mass fractions were calculated as a function of initial pressure (P) equivalence ratio (Ø), temperature, and water loading. Partial pressures were recorded using a 0–2000 mbar sensor (BOC Edwards ASG (±0.2% FS), resolution 0.1 mbar), with a real-time instrument controller readout, and were used to compare with equivalent calculated values. This was a secondary control to ensure that the correct quantities of liquid H_2O mass had fully

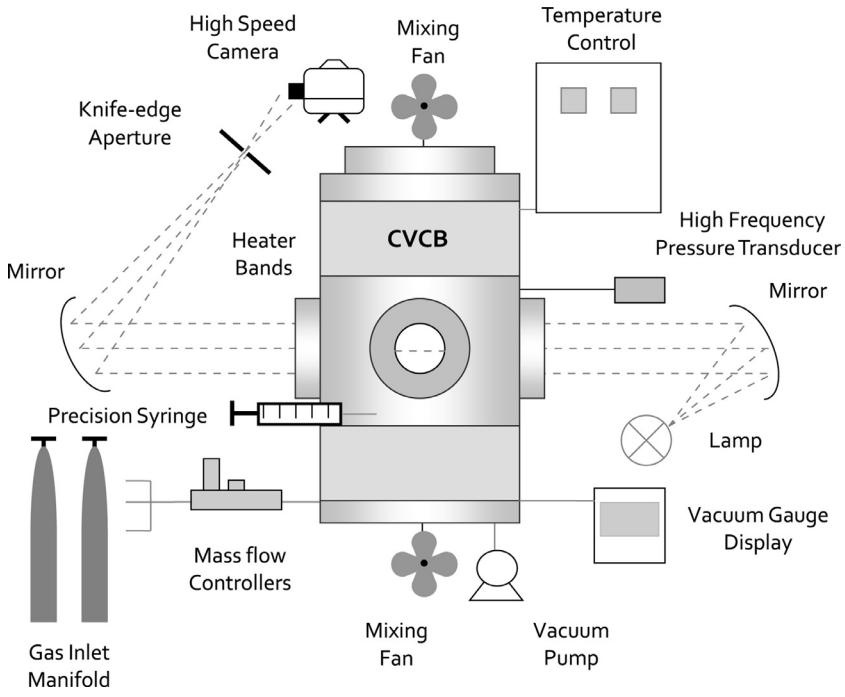

Fig. 2. Schematic overview of the experimental setup.

vaporised, and that required set points had been correctly supplied to the mass flow controllers. A 0–1.2 MPa transducer (GE Unik-5000 (±0.2% FS)) was employed to capture pressure transients resulting from combustion, sampling at a rate of 2 kHz.

Three evacuations of the CVCB were performed between tests; the first to remove products from the previous experiment, followed by two dry compressed air purges to reduce errors arising from imperfect vacuum (<3%, with the remaining air added to the equivalence ratio calculation for each test). Adjacent internal fans were used to blend the fuel, water and oxidant after filling to the required ratio. Capacitor discharge ignition was achieved via fine electrodes mounted at 45° to the plane of measurement, with a variable voltage supply affording control of ignition energy. Experiments were triggered by a simultaneous TTL signal to the ignition and data acquisition systems. A more detailed overview of the mechanical components and benchmarking study has been presented previously [13].

2.2. Fuel composition and experimental conditions

This study was designed to analyse a representative converter gas composition, with increasing levels of pre-vaporised H_2O added to the overall reactant mixture. Fuel fractions were taken from a case study [10], and comprised a molar composition of 66% CO, 19% N_2, 14% CO_2, and 1% H_2. Initial tests were undertaken to simulate change in relative humidity at atmospheric conditions (P = 0.1 MPa, T = 298 K). A range of eight equivalence ratios (calculated from dry air/fuel ratios) was specified from Ø = 0.8 to Ø = 2.2 to determine the peak laminar flame speed, and to quantify any possible enhanced thermo-chemical influence.

Mixture relative humidity (RH) was controlled by injecting a defined mass of liquid H_2O, which was fully vaporised in the chamber, prior to the regulated introduction of fuel and oxidiser. The Antoine equation ($\log_{10}p_v = A_A - B_A/(C_A + T)$ - where p_v corresponds to vapour pressure, and the coefficients of $A_A = 5.402$, $B_A = 1838.675$, and $C_A = -31.737$ for water were obtained from the NIST database [15]) was used to calculate the saturation limit for the specified temperatures, which equated to 0.795 g at 298 K. For the initial atmospheric experiments, four separate levels of H_2O injection were specified in the range of 0–0.6 g, corresponding to a change of ~0–75% RH (at 298 K), or ~2.4%mol of the entire reactant mixture. Full saturation was not tested in order to minimise any possible errors resulting from undesired condensate formation within the vessel. Following chamber evacuation and H_2O injection, complete vaporisation was ensured by monitoring pressure rise within the system. The expected H_2O partial-pressure was subtracted from the specified condition (0.1 MPa), with mass ratios of fuel and air held in proportion for the equivalence ratio specified.

Table 1
Mass of H_2O employed for each experimental condition.

Specified condition								
Temperature (K)	298	298	298	298	323	348	323	348
Pressure (MPa)	0.1	0.06	0.08	0.12	0.1	0.1	0.1	0.1
Mass ratio	**Initial mass** (g)	**H_2O mass for constant ratio (η)** (g)					**H_2O mass for equivalent RH** (g)	
η_A	0.2	0.12	0.16	0.24	0.18	0.17	0.72	2.08
η_B	0.4	0.24	0.32	0.48	0.37	0.34	1.43	4.16
η_C	0.6	0.36	0.48	0.72	0.55	0.51	2.15	6.24

Pressure effects were investigated parametrically using two methods: First, the mass ratio (η) between the fuel and water loading was held constant to analyse the influence of pressure on the flame. The three fuel/H_2O ratios from the stoichiometric atmospheric tests were equivalent to $\eta_A = 0.0124$ $\eta_B = 0.025$ and $\eta_C = 0.0378$, with the respective mass values listed in Table 1. Secondly, mixture water loading was held constant, hence utilising the same H_2O masses injected for the atmospheric 298 K tests (0–0.6 g). Four pressures in the range of 0.06–0.12 MPa were studied, and limited by the concentrations of water vapour achievable at 298 K (for equivalent RH). Similarly, the influence of initial temperature was decoupled in two ways; with both mass ratio of fuel and H_2O held constant (η_A, η_B, and η_C), and the equivalent change in RH (0 to ~75%) for hotter conditions. Initial temperature was increased from 298 K to values of 323 K, and 348 K, with the corresponding mass values listed in Table 1. A stoichiometric fuel/air concentration was chosen, with a minimum of three repetitions to confirm repeatability.

3. Data processing

3.1. Numerical analysis of spherical flames

Results were obtained from the optical system as series of schlieren images depicting the incremental growth of the spherical flame. The shadowed edge was taken to indicate a step change in density - representative of a burned gas isotherm - shown by Giannakopoulos et al. [16] to be critical for characterising the influence of flame stretch. Images were subsequently scaled to determine the 'schlieren radius' (r_{sch}). Limits were set on the range of radii ensuring that both spark influence during early flame growth and effects of pressure increase from the chamber walls, were not influential. Bradley et al. [17] suggested that flame kernels could be spark affected up to a radius of 6 mm for CH_4 flames; however this has been shown to depend on Lewis number [8]. In this study 10 mm was chosen as the minimum radius employed, with preliminary investigations demonstrating minimal variation in results derived from data above 8mm (ignition energy ranged between 55–170 mJ). A maximum usable radius of 35 mm was chosen, based on the calculated limit of 39 mm, corresponding to 30% of chamber radius as proposed by Burke et al. [18]. Using a suitably fast frame capture rate; a minimum of 60 data points (for the fastest flames) were obtained for each test, from which flame speed data were derived.

For an outwardly propagating spherical flame, the stretched flame speed (S_n) is expressed as the temporal (t) derivative of the schlieren flame radius; $S_n = dr_{sch}/dt$. In this study the change in S_n was determined as the regressed differential of the radii plotted against time. The flame stretch rate (α), defined as the change in area (A) gradient as the flame stretches with growth, is calculated for a propagating spherical flame configuration as shown in Eq. (1) [19].

$$\alpha = \frac{1}{A}\cdot\frac{dA}{dt} = \frac{2}{r_{sch}}\cdot\frac{dr_{sch}}{dt} = \frac{2}{r_{sch}}\cdot S_n \tag{1}$$

The quasi-steady nonlinear association between S_n and α [20,21] was employed (rearranged, with the error used for least squares regression) to obtain an extrapolated unstretched flame speed (S_u), as expressed in Eq. (2). The uncertainty in extrapolation was investigated by Wu et al. [22], and for all data presented in this work, the corresponding $Ma_{lin}Ka_{mid}$ values are within the recommended −0.05–0.15 range.

$$\left(\frac{S_n}{S_u}\right)^2\cdot\ln\left(\frac{S_n}{S_u}\right)^2 = -\frac{2L_b\cdot\alpha}{S_u} \tag{2}$$

L_b represents the Markstein Length - as measured relative to the burned gas - and relates change in propagation speed to the influence of flame stretch [20]. Work undertaken by Halter et al. [21] comparing the nonlinear association of atmospheric CH_4/air mixtures demonstrated a strong correlation with the benchmarking work, for both S_u and L_b [10] undertaken using the CVCB. Burned gas expansion must be accounted for in order to obtain values for laminar flame speed (u_L) and at constant pressure is given by Eq. (3).

$$u_L = S_u\cdot\left(\frac{\rho_b}{\rho_u}\right) \tag{3}$$

Adiabatic densities were calculated using CHEMKIN-PRO, employing the chemical reaction mechanism proposed by Davis et al. [23]. The selection of this mechanism is discussed later.

3.2. Quantifying experimental uncertainty

Substantial effort is being made to improve the accuracy of laminar flame speed measurements [8] for mechanism validation, and a detailed approach has been made to quantify uncertainty in the current work (Eq. (4)), using a combination of the experimental facility specification, and accuracy of the processing techniques employed.

$$U_{Su} = \left[\begin{array}{l}\left(\frac{\partial S_u(v_T(\Phi))}{\partial v_T}\cdot y_T\right)^2+\left(\frac{\partial S_u(v_P(\Phi))}{\partial v_P}\cdot y_P\right)^2+\left(\frac{\partial S_u(v_\Phi)}{\partial v_{mo}}\cdot\frac{\partial v_{mo}}{\partial v_\Phi}\cdot y_{mo}\right)^2\\ \quad+\left(\frac{\partial S_u(v_\Phi)}{\partial v_{mf}}\cdot\frac{\partial v_{mf}}{\partial v_\Phi}\cdot y_{mf}\right)^2\\ +\left(\frac{\partial S_u\left(v_{H_2O}(\Phi)\right)}{\partial v_{H_2O}}\cdot y_{H_2O}\right)^2+\left(\left(y_\theta\cdot X_f\cdot 2\cdot S_u\right)+\left(\frac{\partial S_u(v_\Phi)}{\partial\theta}\cdot\frac{\partial\theta}{\partial v\Phi}\cdot y_\theta\right)\right)^2\\ \quad+[(R_{sn}+0.0025_{opt}+0.02_{rad})\cdot S_u]^2\end{array}\right]^{0.5} \tag{4}$$

Uncertainty is quantified for S_u - opposed to u_L - as this is the parameter measured, here defined as U_{Su}. The calculation employs a simplified error propagation methodology to quantify systematic influences by combining the relationship between changes in S_u for several influential variables (v_i, for example T), and the fixed error in each variable (y_i). These uncertainties are comprised of both conditional specification (T, P, Ø, gas purity (θ), and H_2O mass), processing accuracy from the system optics, and nonlinear extrapolation. The potential changes in S_u from several parameters are calculated as a function of Ø; these are temperature (±2 K), pressure (±0.05 kPa), and H_2O concentration (±0.01 g). Data modelled using CHEMKIN-PRO were applied to estimate these profiles wherever experimental results were unavailable. Uncertainty in global equivalence ratio was calculated with respect to the total delivered by each independent mass flow controller (±0.5% Rd), connected to the fuel (mf) and air (mo) supplies, and used to obtain a corresponding change in S_u. It should be emphasised that for simplicity these variables are considered independent in Eq. (4). For example, small changes in Ø will lead to subtle differences in the profiles for S_u change with temperature; however combining these uncertainties results in differences several orders of magnitude lower than the initial independent error - indiscernible on uncertainty plots - and was therefore considered excessive for this analysis.

Uncertainty in S_u resulting from gaseous impurity (θ, specified as ±1% for the given mixture) was calculated as a function of the molar fuel concentration on the basis of several assumptions. First, that any impurity would not influence propagation speed more than a diluent, and secondly, that the influence of flame speed uncertainty scaled directly with 2% of molar fuel fraction (x_f). This is a conservative estimate based upon modelled data for CO_2 and N_2 . In addition, the coupled change in equivalence ratio that results from altering the fuel composition by 1% was also quantified. For this calculation the diluent is modelled as CO_2, to ensure an effective worst-case error in the discrepancy of the mass set point for the target equivalence ratio, due to CO_2 being the densest constituent gas.

Uncertainty resulting from the optical system was calculated from the summated fractional error of both the camera (±2.5/5000 fps), and the spatial resolution of the system (±0.07/35 mm), corresponding to 0.25% of the measured velocity. Moreover, the statistical uncertainty introduced from least squares regression of the nonlinear relationship (R_{sn}) was obtained from a standard method employing residual error [33], and was averaged for all repetitions at a given condition (typically ~2-3%). These uncertainties are applied as a percentage of measured S_u. The uncertainty associated with the nonlinear extrapolation methodology implemented in this research has been investigated previously in the work of Wu et al. [22]. By limiting the usable data range in relation to Markstein and Karlovitz numbers ($Ma_{lin}Ka_{mid}$), the uncertainty from nonlinear extrapolation can be minimised, with all data obtained presented within the range −0.05–0.15.

Radiative heat loss also influences the measured flame propagation [24–26], through a combined influence on both the flame and the calculated density ratio. Here an attempt is made to compensate for this source of error in the calculation of uncertainty. Yu et al. [26] developed an empirical relationship that can be applied to quantify the influence of radiation on spherical flame growth. Unfortunately the derived relationship does not apply when there is re-absorption

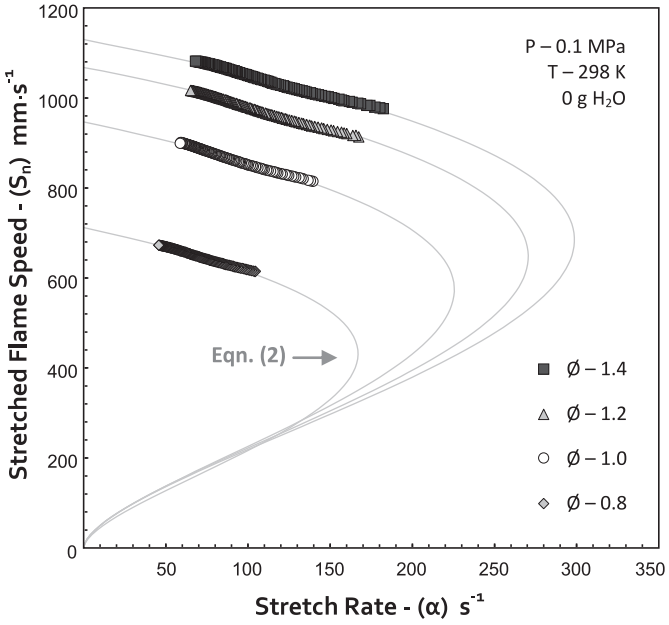

Fig. 3. Examples of S_n plotted against α for dry syngas/air combustion, Ø = 0.8–1.4.

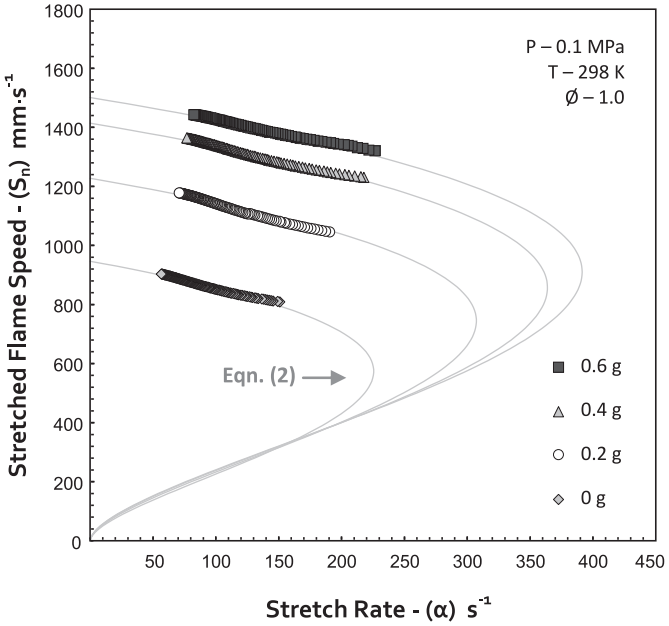

Fig. 4. Examples of S_n plotted against α for syngas/air combustion, 0–0.6 g H_2O (0–75% RH at 298 K).

resulting from the presence of CO_2 in the reactant mixture, and is shown to reduce radiation-induced reduction in flame speed (in addition to CO, which is also discussed). To account for this potential loss, a 2% uncertainty has been added to the U_{su} calculation. This estimate follows the variation presented by Yu and co-workers [26], when CO_2 is added to their applied mixture. Although results are presented for experiments undertaken with CH_4, radiative influence is shown to be fuel independent, and actually a function of propagation speed, with the majority of results in this work falling in the equivalent normalised range ((12–35 cm s^{-1})) to those presented in the reference. In addition, it should also be noted that the influence of buoyancy was assumed to be negligible, with few conditions resulting in speeds below the threshold value of 15 cm s^{-1} suggested by Chen [8]. Flame sphericity was analysed for the few tests that provided results slower than this, and was shown to have negligible effect.

The corresponding uncertainty in the measured laminar flame speed (U_{uL}) was calculated by scaling the error in U_{su} with respect to the density ratio (which was not considered further in the uncertainty analysis). Error bars presented on all subsequent plots are derived from Eq. (4).

Whilst results are also presented here for change in Markstein length, a corresponding uncertainty analysis has not been undertaken. This is because it was difficult to quantify any potential change in the isotherm selected for analysis from the schlieren system employed, known to be influential in measuring L_b [16]; although it should be emphasised that this is independent of measured S_u. Hence the limited number of L_b results presented are assumed – as for most other published work - to be taken from consistent isotherms measured from the burned gas (from consistency in the specified analytical parameters, and optical thresholds in flame edge detection), and are suitable only for general qualitative analysis.

4. Results and analysis

4.1. Atmospheric conditions

Results were obtained as a series of scaled pixel counts, representing incremental growth of the spherical flame radius. Data was processed using the methodology outlined in Section 3.1. Figure 3 shows the effect of dry equivalence ratio (for comparison each data point is visualised from the differential of a third order polynomial fitted to the dr_{sch}/dt curve, with the regressed nonlinear relationship from Eq. (2) superimposed in grey). Extrapolated intercepts on the S_n axis correspond to speeds of zero stretch rates, or the effective unstretched flame speeds, S_u. Data are extracted from the recommended range [22], and do not account for the potential presence of instabilities at low stretch rates. There is an expected offset in the data as S_u values increase with Ø (richer values have been omitted to avoid data overlap).

Trends evident in Fig. 4 suggest similar behaviour to a change in Ø, again with the nonlinear relationship from Eq. (2) superimposed, however this time resulting from addition of H_2O to a stoichiometric mixture. It is clear that this increase in water loading provides a significant offset in the measured value, larger than the absolute differences observed in Fig. 3. It is also evident that the relative offset in measured speed decreases for an equivalent increase in water fraction of 0.2 g. This suggests any thermo-chemical enhancement from the change in humidity decreases with further water addition, and is consistent with analogous data from other studies [1].

The gradients of the data plots reflect the sensitivity of flame speed to a change in stretch rate, characterised by L_b. There is little difference in the gradient of all data sets shown in Figs. 3 and 4, with a negligible change in the trends for an increase in either Ø or water loading. This is represented by a change in L_b for all atmospheric data plotted in Fig. 5, where points show the averaged data for each experimental condition. The level of relative fluctuation in L_b between each repeat was large and whilst all positive values suggest preferential thermal diffusion, there is an ostensible tendency for decreasing L_b with an increase in both Ø and humidity.

This suggests a relative increase in mass diffusivity of the deficient reactant, as expected with the decrease in Lewis number. However, it should be emphasised that the total observed changes are small (~0.4 mm) over the experimental range, with assumed consistency in the isotherm selected for analysis. The flame is therefore only weakly influenced by stretch relative to other fuels mixed with air, such as iso-octane [27], and not significantly changed with the applied concentrations of water.

Extrapolated S_u values have been similarly plotted in Fig. 6, with averages superimposed on the results from all individual experiments. This emphasises the far better repeatability of S_u measurements when compared against L_b, and again shows the rise in flame

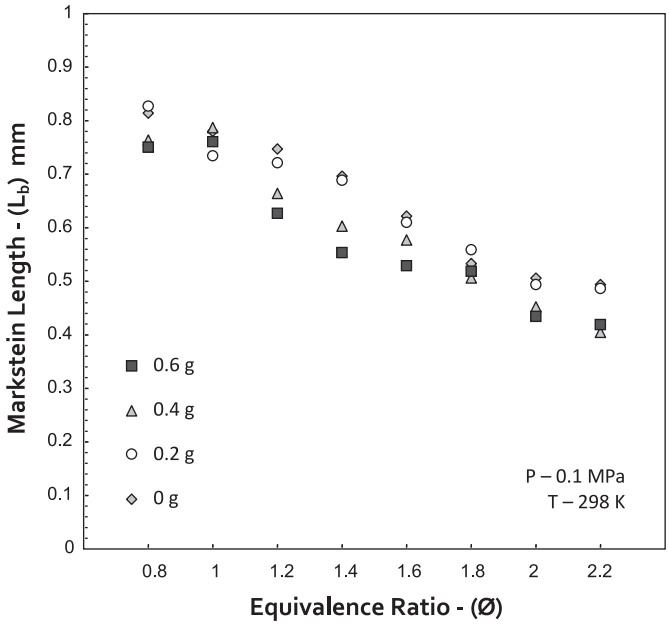

Fig. 5. Variation in average L_b against change in Ø, with an increase in relative humidity 0–0.6 g H_2O (0–75% RH).

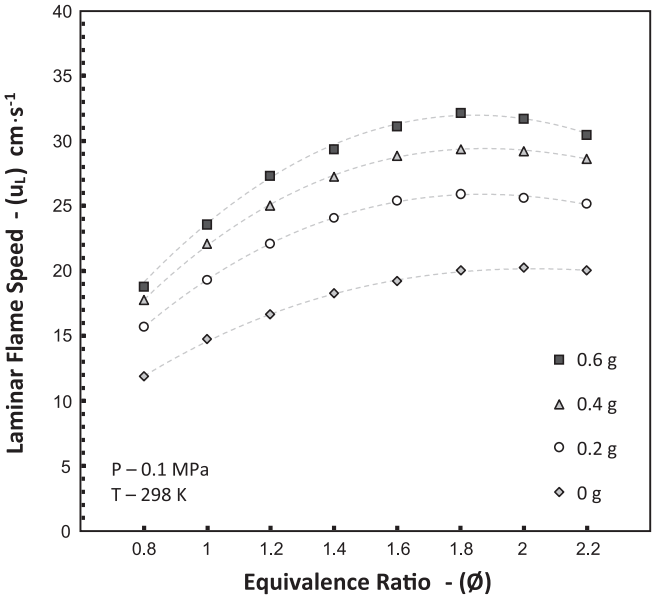

Fig. 7. Variation in u_L against change in Ø, with an increase in relative humidity 0–0.6 g H_2O (0–75% RH). Error bars represent $\pm U_{uL}$.

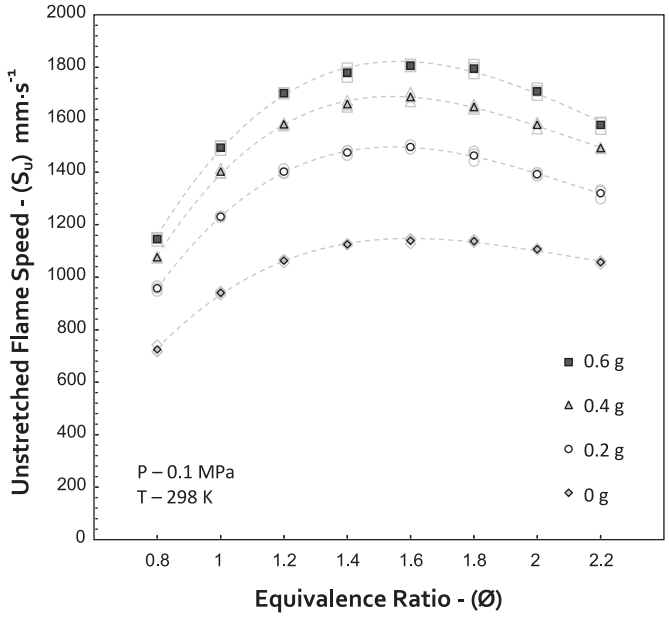

Fig. 6. Variation in S_u against change in Ø, with an increase in relative humidity 0–0.6 g H_2O (0–75% RH). *(Results from all experiments, dark averages superimposed).*

speed resulting from an increase in water loading. Near equivalent percentage increases in S_u values are observed with water addition, a tendency also apparent when corresponding u_L data are generated, as shown in Fig. 7, where $\pm U_{uL}$ is represented by the error bars. For these data, the density ratio was modelled using the Davis et al. [23] mechanism in CHMEKIN-PRO. A sensitivity analysis was performed using different mechanisms [28,29], in addition to the CEA equilibrium code [30] with results varying by <1%.

There are two competing influences on flame propagation: First, a predictable suppressive effect whereby H_2O acts as a diluent and speed is slowed by a reduction in flame temperature. The second influence results from changes in flame thermochemistry, and an increase in overall reaction rate due to the changes in the dissociative production of chain carrying species, and enhanced heat release rate. The catalysing effect of these radicals on CO consumption processes have been shown to reduce the slow reaction (with high activation energy): $CO + O_2 \rightarrow CO_2 + O$ [1,9]. The enhancement in production of carriers is reduced as water concentration increases, and is counteracted by the suppressive effect of H_2O as a diluent.

The results from chemical kinetic models have been plotted in Fig. 8 to provide a visual demonstration of this effect. PREMIX was utilised by CHEMKIN-PRO together with the reaction mechanism developed by Davis et al. [23] comprising 14 chemical species and 38 reactions. Solutions are based on an adaptive grid of 1000 points with mixture-averaged transport properties and trace series approximation to model combustion for three equivalence ratios (Ø = 1, 1.4, and 1.8). Figures 8a and b show the respective maximum molar fractions of OH and HCO from the predicted 1-D spatial concentration profiles. Averaged experimental flame speed data have been scaled and superimposed to provide examples of the analogous trends in the results. It is also evident that an increase in Ø provides a relative decrease in maximum OH, contrasted against a rise in HCO. This is as a result of the change in relative abundance of O and C as the reactant mixture gets richer. The addition of H_2O is shown to enhance the concentrations of both species through dissociative production.

Figure 8c shows the resultant change in maximum net heat release rate (HRR), with predicted values again demonstrating a similar trend to experimental u_L. This results from the increased production of intermediate species enhancing CO oxidation, and is counteracted by a reduction in T_{AD} from H_2O as a diluent (Fig. 8d). This counteracting behaviour is non-monotonic, and if the fuel blend contained a higher H_2 fraction, carriers would be inherently produced from an increase in reactions such as: $CO + H_2 \rightarrow H + HCO$. Hence, the accelerative influence of H_2O diminishes, T_{AD} suppression is dominant, and enhancement in laminar flame speed reduces.

It should be emphasised that the observed variation in flame behaviour is significant compared to the small change in reactant composition (~2.4%mol), and is likely to occur with the practical application of utilising converter gas under different atmospheric conditions. It is therefore likely that change in humidity could lead to premixed instabilities, such as lean blow off or flashback [31], and it is suggested that atmospheric fuel/air mixtures could be saturated with water vapour to possibly improve operational performance. In doing so, the effect of any fluctuations in fuel composition (particularly H_2)

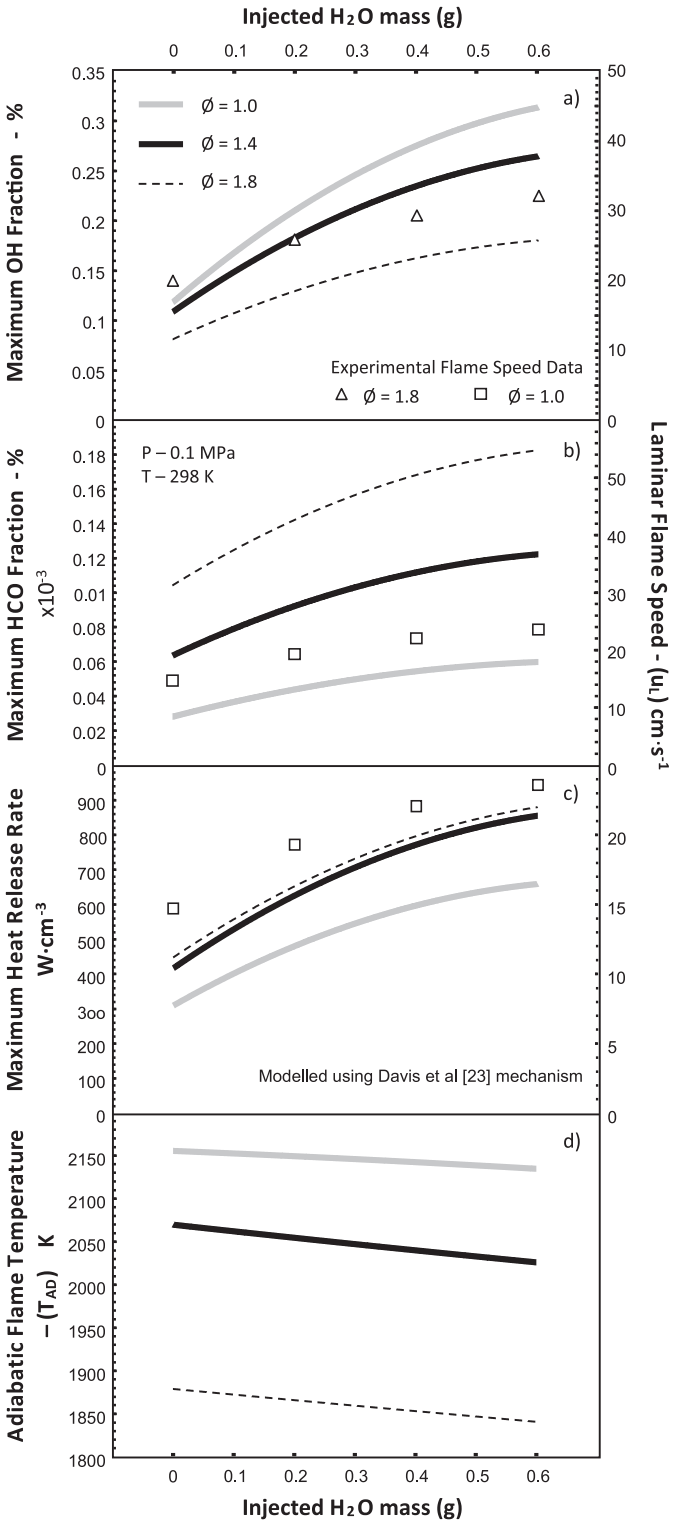

Fig. 8. Change in modelled parameters against relative humidity for 3 equivalence ratios, with experimental u_L superimposed. (a) Maximum OH fraction. (b) Maximum HCO fraction. (c) Maximum heat release rate. (d) Adiabatic flame temperature T_{AD}.

could also be reduced. These results also highlight water vapour as a potential source of error in the experimental measurement of u_L, significant for fuels with a large CO component.

4.2. Influence of temperature

As outlined in Section 2.2, initial experiments were performed at temperatures of 298, 323 and 348 K, keeping three mass ratios

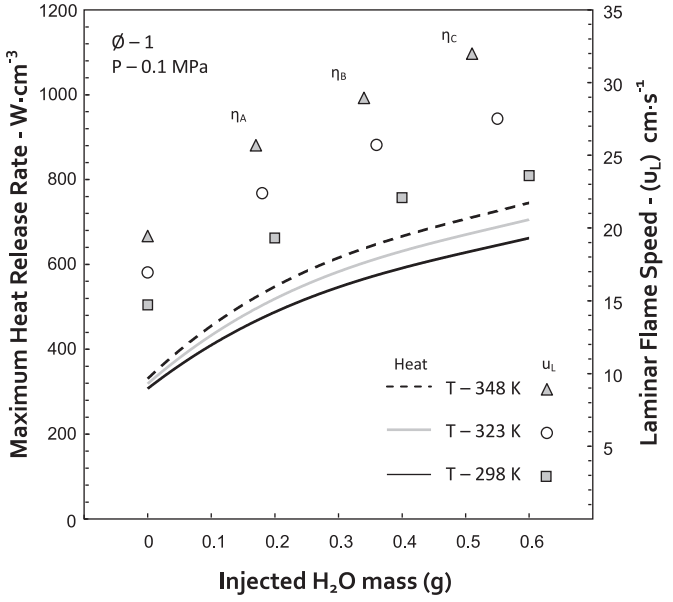

Fig. 9. Variation in u_L and maximum heat release rate against constant H_2O/fuel mass ratios with an increase in T (298–348 K).

Table 2
Percentage normalised change in condition from water/fuel ratio η_C to dry case.

T	Change in u_L (%)	Change in T_{AD} (%)
298	60.3	−0.97
323	62.5	−0.95
348	64.4	−0.99

(η_A, η_B, and η_C) of fuel/H_2O constant, in order to study the influence of temperature on catalytic H_2O induced flame propagation increase. In doing so, the molar fractions of intermediate carrier production, and subsequent increase in heat release rate were varied from the initial thermal specification. Results for constant fuel/water ratios were obtained for stoichiometric conditions and are shown in Fig. 9, with corresponding u_L values as well as maximum HRR plotted against water mass. Density ratios and HRR predictions were obtained using the Davis et al. [23] mechanism. Similar trends are again evident between change in u_L and HRR, with values ostensibly increased in proportion from the initial dry tests. Percentage normalised changes in u_L from dry to the maximum water loading case are listed in Table 2 for each T, in addition to the change in T_{AD}.

Experimental results suggest a relative increase in the normalised change in u_L from an equivalent rise in H_2O addition with temperature. This may result from the disproportionate decrease in T_{AD} (consistently ~20 K, or around 1% from Table 2) from the dry mixtures, to those comprising largest H_2O fractions; not changing at the same rate as intermediate species formation, and subsequent increase in HRR (as shown in Fig. 9). It can be observed that temperature appears to enhance the catalytic influence of H_2O addition on u_L, perhaps by increasing the influence of change in HRR and effectively reducing the influence of the drop in T_{AD}. Further experiments could be performed to support this explanation, diluting the mixture to have equivalent values of T_{AD} for changes in specified temperature. However, it should be noted that the measured changes are small - encompassed within the experimental uncertainty of the system - and whilst chemical models agree with this observation, further testing is required for validation at higher temperatures.

The increase in vapour pressure that results from temperature rise allows for larger H_2O fractions in the reactant mixture. Further stoichiometric experiments were performed, increasing water fraction to

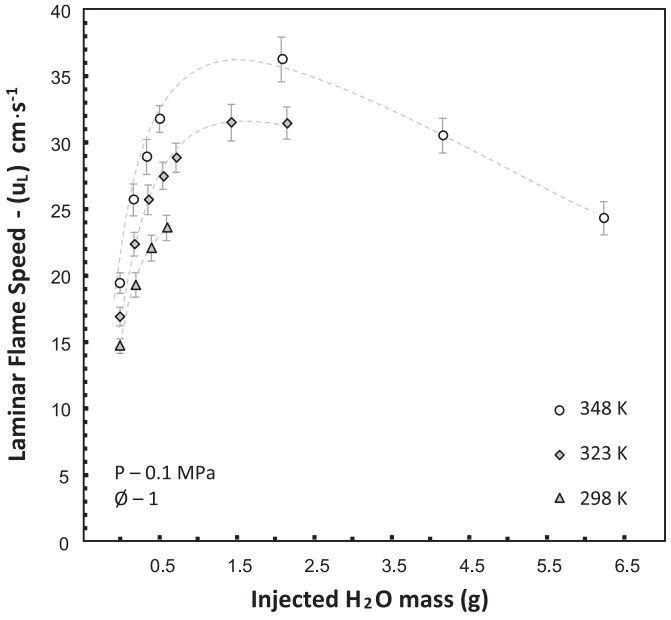

Fig. 10. Variation in u_L against H_2O mass for all experimental data with an increase in T (298–348 K) Error bars represent $\pm U_{uL}$.

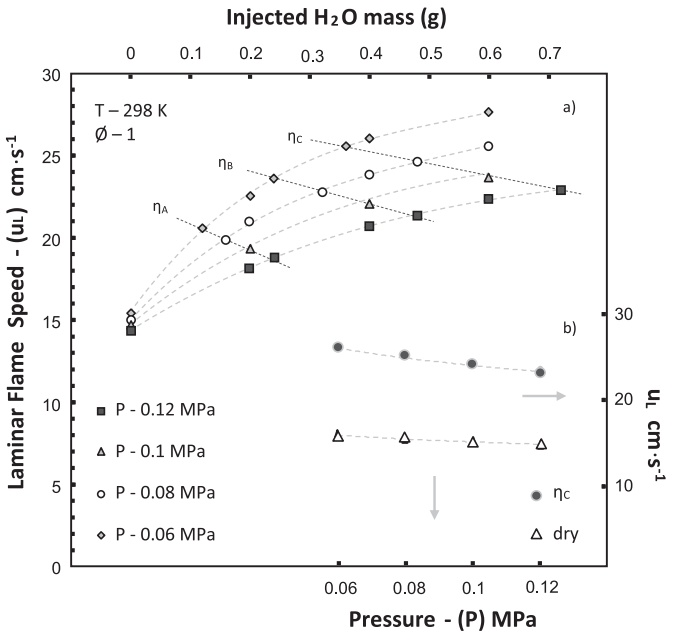

Fig. 11. (a) Variation in u_L against H_2O mass with an increase in P (0.06–0.12 MPa): constant mass ratios and RH. (b) Examples of changes in measured u_L with an increase in P Error bars represent $\pm U_{uL}$.

maintain values of relative humidity (~25, 50, and 75%) at elevated temperatures. These data are plotted in Fig. 10, in addition to values obtained for constant fuel/water ratio. A non-monotonic influence of water loading increase is observed in agreement with other studies [1–3], with initial acceleration in the measured speeds slowed, and eventually reversed for the hottest tests. At 348 K, the wettest condition corresponds to an overall H_2O fraction of ~28.7%mol in the reactant mixture, with the suppressive effect of H_2O as a diluent reducing T_{AD} by over 20%, and the peak HRR nevertheless remaining higher than the equivalent dry tests. When compared to other data [1,13], the maximum H_2O concentration achieved prior to a reduction in u_L appears to be a function of initial CO/H_2 ratio, with the catalytic influence lessened for an increase in H_2 and subsequent formation of chain carrying species.

4.3. Influence of pressure

The influence of pressure was studied over a restricted range (0.06–0.12 MPa), due to the limitations imposed by H_2O vapour pressure achievable at 298 K. Nevertheless, the specification employed allowed for analysis of the influence of pressure in the same way as temperature; keeping the mass ratios of fuel/water constant (i.e. η_A, η_B, and η_C, with the values listed in Table 1). Experiments were also performed with equivalent H_2O mass loadings to the original atmospheric tests, corresponding to equivalent vapour pressures, as temperature was held constant at 298 K. Measured stoichiometric u_L values are plotted for each pressure against water mass in Fig. 11a, where dashed lines have been superimposed for greater clarity. Similar tendencies are observed for all pressures considered, with an increase in H_2O mass again yielding diminishing enhancements in u_L.

The relative normalised change in u_L from each dry condition is plotted against pressure in Fig. 12, with trend lines superimposed. A decreasing tendency is observed for all mass ratios, suggesting an increase in pressure reduces the catalytic enhancement of H_2O addition on u_L (note the observed changes are again small, so the results of individual tests have been provided in grey to give an indication of experimental scatter). This apparent reduction is again attributed to the relative change in carrier production, and subsequent HRR, resulting from an increase in pressure. To demonstrate this, H_2O induced change in T_{AD} and the maximum modelled HRR have been

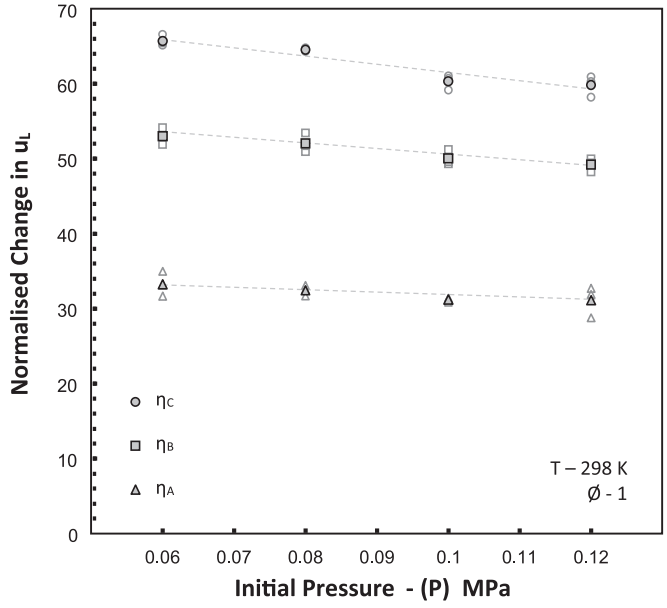

Fig. 12. Normalised change in u_L for each tested condition against change in corresponding P. (uLnc - uLdry)/(uLdry) × 100%.

normalised against the equivalent dry condition (X_η/X_{dry} with values again obtained using the Davis et al. [23] mechanism), and plotted for the highest and lowest pressures in Fig. 13. A rise in P is shown to reduce the normalised increase in HRR, and by a larger amount than T_{AD}. This is in contrast to the tendency shown for change in temperature, and hence why the opposite effect is observed.

Offsets in u_L are evident for different pressures when maintaining RH as a function of change in fuel/H_2O ratio. For instance, an increase in RH of 25% results in a larger equivalent change in u_L for an initial pressure of 0.06 MPa compared to 0.1 MPa, due to increased water vapour relative to the amount of fuel, and hence widening of the trend lines shown in Fig. 11a. In addition, the data has been analysed from the opposing perspective, with change in u_L observed as a

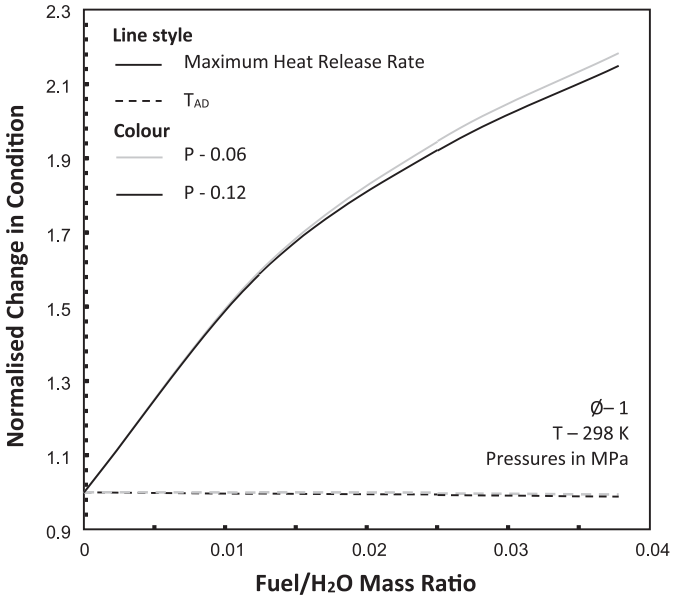

Fig. 13. Normalised change in maximum heat release rate and T_{AD} for two experimental pressures (0.06 and 0.12 MPa).

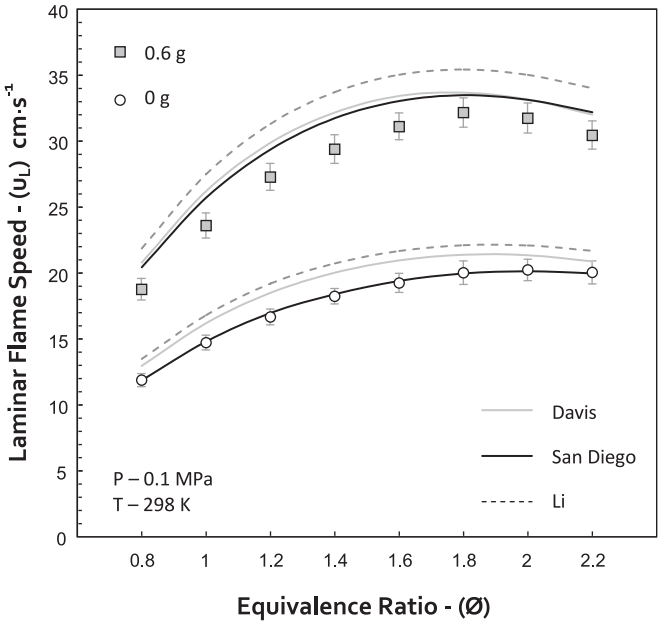

Fig. 14. Atmospheric experimental and modelled data comparison using published reaction mechanisms. Error bars represent $\pm U_{uL}$.

function of P for each test composition. Power law correlations were derived (as described elsewhere [32]), and show a decrease in exponents from −0.103 for the dry dataset to −0.161 for η_C. Therefore an increase in P provides a larger reduction in u_L for humid mixtures, with reduced chain carrier production, and hence the subtle change in the gradient of data plotted in Fig. 11b.

4.4. Reaction mechanism analysis

An initial comparison was made between the atmospheric experimental data and values modelled with three reaction mechanisms, using the PREMIX coded laminar flame speed calculator in CHEMKIN-PRO: The Davis [23] mechanism previously employed in the study (14 chemical species, 38 reactions), the modified Li et al. [28] mechanism with C1 species (21 in total, in 93 reactions) and the San Diego mechanism (46 chemical species, 235 reactions) by Petrova and Williams [29]. Again, solutions were based on an adaptive grid of 1000 points with mixture-averaged transport properties and trace series approximation. These mechanisms are chosen as they were shown to model moist syngas combustion with a favourable correlation against experimental data [2]. Results are plotted in Fig. 14 with only the 0 g and 0.6 g H_2O mass loading data plotted for greater clarity. The San Diego mechanism demonstrates good agreement with the driest tests. However, all models provide an overprediction in u_L for the humid mixtures, with an error margin of over 15% for the worst cases. This tendency has been shown in other work, and is attributed to the modelled underproduction of H_2O with OH when water concentrations are elevated. Das et al. [1] used a sensitivity analysis to demonstrate the significance of the chain branching reaction $OH + H_2 = H_2O + H$ when modelling humid syngas combustion with low concentrations of H_2. Moreover, the comparative significance of OH consumption with the branching reaction $OH + OH = O + H_2O$ is also emphasised by the authors for humid, low H_2 mixtures. Initially using the Davis mechanism as a framework, an adaptation to the rate parameters of these two equations has been made and is presented in Table 3, identified as R1 and R2 respectively.

The pre-exponential factor for R1 has been increased by an order equivalent to the San Diego mechanism, with a corresponding rise in activation energy. Conversely, the equivalent A factor for R2 is reduced to a third order constant. An equivalent comparison made between the atmospheric experimental data and modified Davis mechanism (MDM) is shown in Fig. 15. It should be noted that other reactions were analysed, but changing these two resulted in the most favourable comparison between the modelled an experimental data.

Table 3
Changes made to the rate parameters ($k = AT^n \exp(-E/RT)$) of two equations in the Davis mechanism [23].

Reaction	A	n	E	Identifier
$OH + H_2 = H + H_2O$	1.734 E + 9	1.510	3635.00	**(R1)**
$OH + OH = O + H_2O$	3.973 E + 03	2.400	−2110.00	**(R2)**

Changing the rate parameters of the two specified equations is shown to result in a closer agreement between the modelled and experimental data for both the 0 g and 0.6 g H_2O loading conditions. This results from an increase in the consumption of OH carriers in the stated branching equations, and a rise in H_2O production. These tendencies can be seen on the plotted spatial concentration profiles shown in Fig. 16. A comparison is given between the MDM and San Diego (best performing of the three employed) mechanisms, for both the 0 g and 0.6 g H_2O cases. Minimal difference is predicted between the H_2O and OH profiles for the 0 g case. By contrast, a respective rise and fall in production from the MDM scheme is evident for the humid mixture. The resultant change in heat release rate slows the overall reaction, reducing u_L to a more representative value. In addition, there is an offset in the HCO profiles shown for each case, with an increased number of HCO reactions in the more detailed San Diego mechanism. The subtle changes in species production with axial distance should be verified with measured concentration profiles.

The performance of the MDM was assessed further for change in initial condition, with a comparison between the San Diego predictions and experimental results at elevated T and P presented in Fig. 17. Close agreement is noted at the driest conditions for both mechanisms, however favourable agreement is shown for the MDM as the mixture humidity rises, with an analogous overprediction from the San Diego data. As a further validation of the MDM, a comparison is also made against the published data of Das et al. [1] shown in Fig. 18. The lowest values correspond to an $\eta_{H2/CO}$ ratio of 0.053, and the highest 0.25 (5/95% and 20/80% respectively)

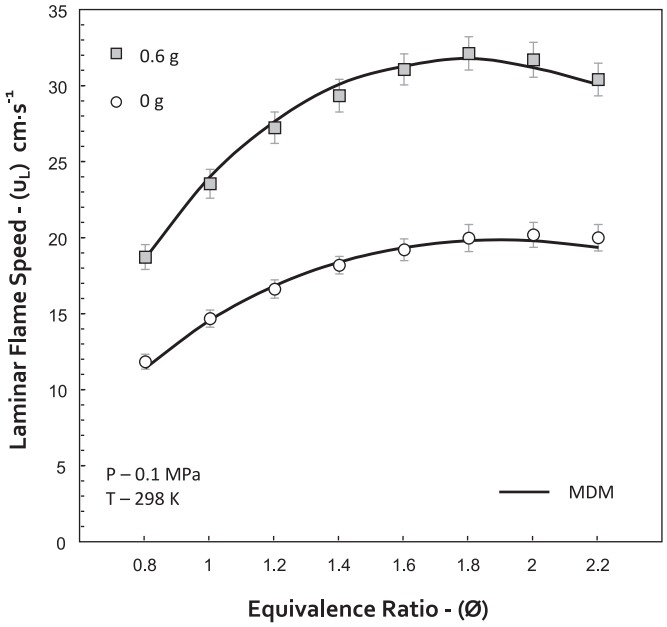

Fig. 15. Atmospheric experimental and modelled data comparison using the modified Davis mechanism (MDM).

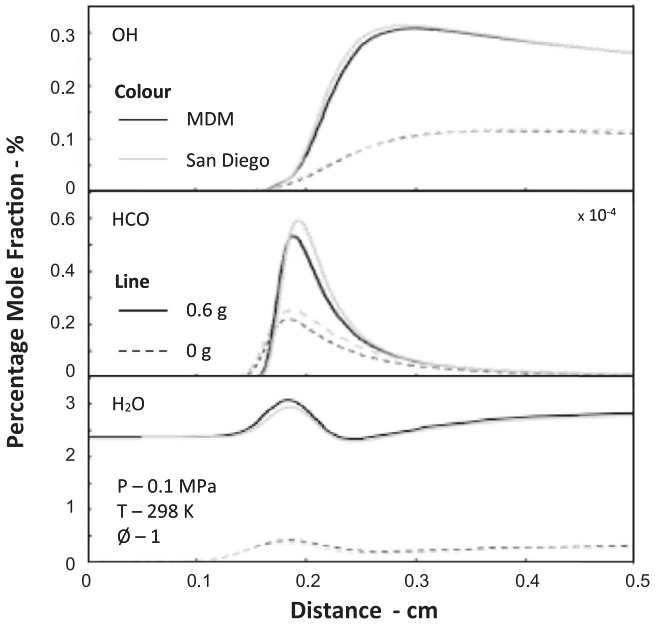

Fig. 16. Spatial concentration profiles for OH, HCO, and H2O in a 1-D flame modelled using CHEMKIN-PRO with MDM and San Diego mechanisms.

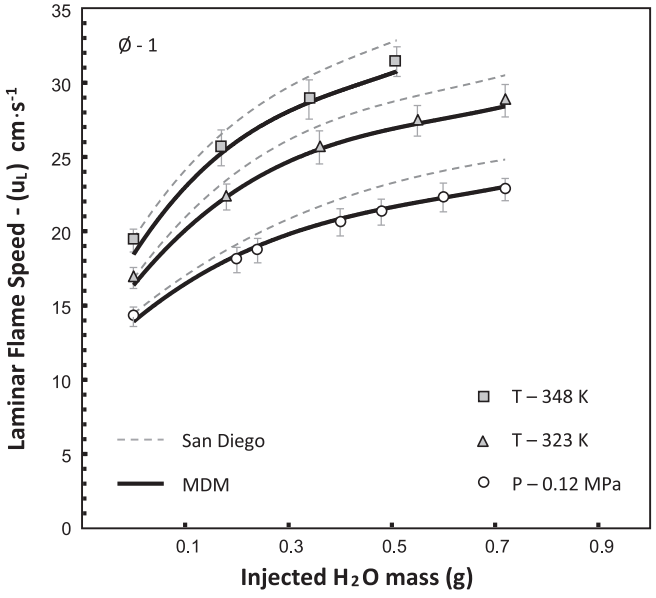

Fig. 17. Experimental and modelled u_L data comparison for elevated temperature and pressures.

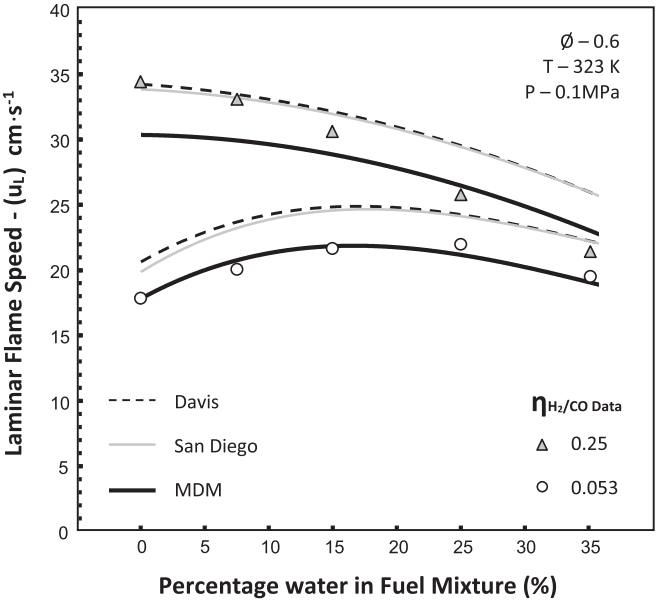

Fig. 18. Experimental and modelled data comparison using results from Das et al. [1], with the San Diego, and both original and modified Davis mechanisms.

with H_2O fraction increased as a percentage of the fuel mixture. Good agreement between the MDM and the $\eta = 0.053$ data is demonstrated for all water loadings, whereas the Davis and San Diego mechanisms consistently overpredict the equivalent u_L data. However the accuracy of the MDM is reduced as the H_2 fraction is increased for the driest conditions, and only begins to correlate favourably against the $\eta_{H2/CO} = 0.25$ dataset for H_2O fractions greater than 15%. Results therefore suggest that the MDM is suitable for modelling combustion of humid syngas mixtures, with initially high CO/H_2 or H_2O/H_2 ratios, to account for the suppressive influence of chain branching reduction, and intermediate H_2O increase. However, further work is required to assess the performance of the MDM at higher conditions of combined temperature and pressure.

5. Conclusions

– A small increase (~2.4%mol of overall reactant composition) in water concentration has been shown to have a substantial impact on measured laminar flame speed for a practical syngas: Increases in flame speed of up to 70% have been realised. This increase results from the dissociative influence of H_2O addition, forming chain carriers that catalyse the oxidation of CO, and enhance heat release rate. This accelerative influence diminishes for the higher water loadings, as it is countered by a lowering of adiabatic flame temperature from H_2O acting as a diluent. Changes in relative humidity could therefore induce practical instabilities such as lean blow off for premixed fuels, and it is suggested that saturating relevant fuel/air mixtures with water vapour at atmospheric conditions may improve operational stability.

- The influence of initial temperature on H_2O induced flame speed increase was investigated; holding the mass ratios of fuel and H_2O constant for a step change in condition. Changes in modelled adiabatic flame temperature were shown to be weaker than the catalytic increase in heat release rate, with greater relative acceleration associated with elevated initial conditions. Further increase in reactant H_2O fraction eventually results in the non-monotonic influence observed previously, with flame speed peaking before eventually decreasing. The relative change in flame speed, and maximum H_2O concentration prior to deceleration are shown to be a function of initial CO/H_2 ratio.
- The effect of initial pressure was investigated also, with the opposite influence compared with the temperature effect observed: A greater relative decrease in heat release rate and adiabatic flame temperature suppresses the catalytic influence of H_2O addition, thereby slowing flame propagation. This combined influence also results in a more substantial change in flame speed as a function of initial pressure, with humid mixtures slowing by a greater amount at elevated conditions. Constant relative humidity is shown to provide an offset in flame speed at different pressures, as a function of the fuel/H_2O ratio.
- The performance of several published reaction mechanisms were assessed against the CVCB data; a consistent overprediction in flame speed is evident when H_2O is added to the mixture. Hence, a modified reaction mechanism (MDM) has been developed based on the work of Davis et al. [23], and is presented for the humidified combustion of high CO/H_2 mixtures. After some sensitivity analysis, the MDM is derived by modifying the rate parameters of two dominant chain branching reactions: $OH + H_2 = H_2O + H$ and $OH + OH = O + H_2O$, to give higher relative indeterminate H_2O formation, and a reduction in OH carriers. Results obtained using the MDM demonstrate considerably improved performance against all CVCB data, including tests performed at elevated temperatures and pressures. The mechanism also compares favourably with high CO/H_2 data published previously, with the largest discrepancy associated with an increase in H_2 fraction occurring at the driest conditions.
- The results also highlight relative humidity as a potential source of error in the experimental measurement of u_L, particularly significant for fuel mixtures comprising large CO fractions. With increased emphasis on the accurate determination of laminar flame speed, H_2O fraction should therefore be carefully controlled to ensure accuracy of data. A methodology employed for estimating experimental uncertainty is described, implemented and presented in a selection of data plots throughout this paper.

Acknowledgements

This work has resulted from an interdisciplinary research programme partially funded the Low Carbon Research Institute (Welsh European Funding Office, Grant 80366), and Cardiff University's Gas Turbine Research centre (GTRC).

References

[1] A.K. Das, K. Kumar, C.J. Sung, Laminar flame speeds of moist syngas mixtures, Combust. Flame 158 (2011) 345–353.
[2] Y. Xie, J. Wang, N. Xu, S. Yu, M. Zhang, Z. Huang, Thermal and chemical effects of water addition on laminar burning velocity of syngas, Energ. Fuel 28 (2014) 3391–3398.
[3] D. Singh, T. Nishiie, S. Tanvir, L. Qiao, An experimental and kinetic study of syngas/air combustion at elevated temperatures and the effect of water addition, Fuel 94 (2012) 448–456.
[4] Y. Xie, J. Wang, N. Xu, S. Yu, Z. Huang, Comparative study on the effect of CO_2 and H_2O dilution on laminar burning characteristics of CO/H_2/air mixtures, Int. J. Hydrogen Energ. 39 (2014) 3450–3458.
[5] J. Santner, F. Dryer, Y. Ju, Effect of water content on syngas combustion at elevated pressure, 50th AIAA Aerospace Sciences Meeting, (2012), paper AIAA 2012-0163.
[6] C.K. Law, Combustion physics, Cambridge University Press, 2006.
[7] IPPC european commission, Best available techniques reference document on the production of iron and steel, industrial emissions directive 2010/75/EU 2013.
[8] Z. Chen, On the accuracy of laminar flame speeds measured from outwardly propagating spherical flames: Methane/air at normal temperature and pressure, Combust. Flame 162 (2015) 2442–2453.
[9] D. Pugh, A. Crayford, P. Bowen, T. O'Doherty, R. Marsh, Variation in laminar burning velocity and Markstein Length with water addition for industrially produced syngases, ASME Turbo Expo 2014 (2014), paper GT2014-25455.
[10] D. Pugh, Combustion characterisation of compositionally dynamic steelworks gases, Cardiff University, 2014 PhD thesis.
[11] A. Bouvet, C. Chauveau, I. Gokalp, F. Halter, Experimental studies of the fundamental flame speeds of syngas (H_2/CO)/air mixtures, Proc. Comb. Inst. 33 (2011) 913–920.
[12] T. Tahtouh, F. Halter, E. Samson, C. Mounaïm-Rousselle, Effects of hydrogen addition and nitrogen dilution on the laminar flame characteristics of premixed methane–air flames, Int. J. Hydrogen Energ. 34 (2009) 8329–8338.
[13] D. Pugh, T. O'Doherty, A. Griffiths, P. Bowen, A. Crayford, R. Marsh, Sensitivity to change in laminar burning velocity and Markstein length resulting from variable hydrogen fraction in blast furnace gas for changing ambient conditions, Int. J. Hydrogen Energ. 38 (2013) 3459–3470.
[14] T. Tahtouh, F. Halter, C. Mounaïm-Rousselle, Measurement of laminar burning speeds and Markstein lengths using a novel methodology, Combust. Flame 156 (2009) 1735–1743.
[15] NIST chemistry web-book. < http://webbook.nist.gov/chemistry/ >. Accessed 10/12/2014.
[16] G.K. Giannakopoulos, A. Gatzoulis, C.E. Frouzakis, M. Matalon, A.G. Tomboulides, Consistent definitions of "Flame Displacement Speed" and "Markstein Length" for premixed flame propagation, Combust. Flame 162 (2015) 1249–1264.
[17] D. Bradley, P.H. Gaskell, X.J. Gu, Burning velocities, markstein lengths, and flame quenching for spherical methane-air flames: a computational study, Combust. Flame 104 (1996) 176–198.
[18] M. Burke, Z. Chen, Y. Ju, F. Dryer, Effect of cylindrical confinement on the determination of laminar flame speeds using outwardly propagating flames, Combust. Flame 156 (2009) 771–779.
[19] D.R. Dowdy, D.B. Smith, S.C. Taylor, The use of expanding spherical flames to determine burning velocities and stretch effects in hydrogen/air, Symp. (Int.) Combust. 23 (1991) 325–332.
[20] A.P. Kelley, C.K. Law, Nonlinear effects in the extraction of laminar flame speeds from expanding spherical flames, Combust. Flame 156 (2009) 1844–1851.
[21] F. Halter, T. Tahtouh, C. Mounaïm-Rousselle, Nonlinear effects of stretch on the flame front propagation, Combust. Flame 157 (2010) 1825–1832.
[22] F. Wu, W. Liang, Z. Chen, Y. Ju, C.K. Law, Uncertainty in stretch extrapolation of laminar flame speed from expanding spherical flames, Proc. Combust. Inst. 35 (2015) 663–670.
[23] S.G. Davis, A.V. Joshi, H. Wang, F. Egolfopoulos, An optimized kinetic model of H2/CO combustion, Proc. Combust. Inst. 30 (2005) 1283–1292.
[24] J. Santner, F.M. Haas, Y. Ju, F.L. Dryer, Uncertainties in interpretation of high pressure spherical flame propagation rates due to thermal radiation, Combust. Flame 161 (2014) 147–153.
[25] C.H. Sohn, Z. Chen, Y. Ju, Effects of radiation on the uncertainty of flame speed determination using spherically propagating flames with $CO/CO_2/H_2O$ dilutions at elevated pressures, Int. J. Heat Mass Tran. 86 (2015) 820–825.
[26] H. Yu, W. Han, J. Santner, X. Gou, C.H. Sohn, Y. Ju, Z. Chen, Radiation-induced uncertainty in laminar flame speed measured from propagating spherical flames, Combust. Flame 161 (2014) 2815–2824.
[27] B. Galmiche, F. Halter, F. Foucher, Effects of high pressure, high temperature and dilution on laminar burning velocities and Markstein lengths of iso-octane/air mixtures, Combust. Flame 159 (2012) 3286–3299.
[28] J. Li, Z. Zhao, A. Kazakov, M. Chaos, F.L. Dryer, A comprehensive kinetic mechanism for CO, CH_2O, and CH_3OH combustion, Int. J. Chem. Kinet. 39 (2007) 109–136.
[29] Chemical-Kinetic Mechanisms for Combustion Applications, San Diego Mechanism web page, Mechanical and Aerospace Engineering (Combustion Research) < http://web.eng.ucsd.edu/mae/groups/combustion/mechanism.html >Accessed 01/12/2014.
[30] S. Gordon, B.J. McBride, Computer program for calculation of complex chemical equilibrium compositions and applications, NASA Reference Publication, 1994, p. 1311.
[31] T. Lieuwen, Unsteady combustor physics, Cambridge University Press, 2012.
[32] X. Gu, M. Haq, M. Lawes, R. Wooley, Laminar burning velocity and Markstein lengths of methane-air mixtures, Combust Flame 121 (2000) 41–58.
[33] H.W. Coleman, W.G. Steele, Experimentation and uncertainty analysis for engineers, 3rd Edition, John Wiley & Sons, 2009.